This is the author's version of an article that has been published in this journal. Changes were made to this version by the publisher prior to publication.
The final version of record is available at http://dx.doi.org/10.1109/TMTT.2014.2359855

Compact Conical Line Power Combiner Design Using Circuit Models

Ryno D. Beyers, *Student Member, IEEE*, and Dirk I. L. de Villiers, *Member, IEEE*

***Abstract*—A simple equivalent circuit model with empirical equations describing the peripheral feeding ports of conical line power combiners is presented. The model allows the entire structure to be designed using transverse electromagnetic circuit theory without the need for any full-wave simulations. A summary of the model extraction process is given and the accuracy of the proposed model is confirmed by favorable comparisons with full-wave simulations. The circuit based design method is used to design a compact conical line combiner showing measured performance similar to the current state of the art combiners in this technology, while being significantly smaller.**

***Index Terms*—Circuit models, combiners, conical combiners, conical transmission lines, N-way splitters, optimization, passive components, radial combiners.**

I. Introduction

AXIALLY symmetric N-way power combiners offer a number of advantages over conventional corporate and chain combiners when N is large. These advantages include higher combining efficiencies due to reduced insertion loss and improved amplitude and phase balance, as well as reduced physical size and weight [1]–[3]. With few exceptions, these types of combiners have traditionally been difficult to design: Electromagnetic field analysis is used in [4], empirical techniques based on measurements is used in [5], and for some others no detailed design information is provided [6]–[8]. With the advent and continued improvement of 3D electromagnetic modeling software, the analyses and simplified design approaches of many variations based on radial, coaxial and conical transmission lines have been presented [9]–[15].

The conical transmission line implementation of N-way power combiners [10] is a relatively new technology offering some advantages over the more conventional coaxial line [12], [16] and radial line [9] structures. The conical combiners in [10] and [11] are designed using a hybrid technique where a minimal number of full-wave simulations are required: Even though conical transmission lines support a fundamental transverse electromagnetic (TEM) mode and may thus be designed by circuit theory, the peripheral ports of conical combiners that transition into the conical lines contain discontinuities where higher order modes are excited, and cannot be modeled by simple TEM transmission lines [17]. Equivalent circuit models have previously been used to model different parts – including in some cases the peripheral port transitions – of various types of combiners. However, most of these circuit models do not offer a means to relate the circuit element values to physical dimensions [12], [18], or they are not accurate enough to be used exclusively and full-wave optimization or parameter sweeps are still needed afterwards to obtain the final dimensions of the structures [9]–[11], [13], [14].

The authors are with the Department of Electrical and Electronic Engineering, University of Stellenbosch, Stellenbosch 7600, South Africa (email: 15407756@sun.ac.za; ddv@sun.ac.za).

This paper presents a set of general empirical equations based on full-wave simulations that describe the circuit model, as presented in [19] and shown in Fig. 1, for shorted coaxial peripheral feeding ports in conical combiners. The empirical equations allow the designer to determine the equivalent circuit element values accurately and directly from the physical dimensions of conical combiners and vice versa. In many cases the empirical equations are accurate enough to allow the circuit model to be used exclusively during the design process, eliminating the need for full-wave analyses. This allows for rapid optimization of various dimensions of the combiner at a significantly reduced computational cost compared to full-wave optimization together with matching networks that may be required for wide band operation. This method also enables the designer to minimize the total transmission length and thus the physical size of the combiner.

The parameter extraction method and the subsequent model derivation are discussed, followed by some example designs using the circuit model. Full-wave simulations of the final structures are performed to confirm the accuracy of the proposed method, where close correlations between the circuit models and the full-wave results are obtained. The proposed circuit based design method is validated by comparing the simulation results of an example design with its measurements.

II. Physical Description And Empirical Equation Extraction

The basic layout of a conical combiner is shown in Fig. 1, where the different regions that will be used in the circuit model description are indicated by dotted boxes. Note that the figure is rotationally symmetric around the vertical axis on the left. The equivalent circuit model for the combiner and the location of external matching networks that may be added is shown in Fig. 2, where the equivalent circuit for each region of the combiner is contained within its corresponding box. The peripheral feeding port transition used here is the uncompensated version without tuning posts, as defined in [19], and is different from what is used in [10] and [11]. Note that the circuit model is only valid for the symmetrically driven case where the fields at the peripheral input ports have the same amplitude and phase. In Fig. 1, regions A and F are coaxial lines, regions C and E are conical lines, and region B is a constant impedance conical to coaxial line

Copyright (c) 2014 IEEE. Personal use is permitted. For any other purposes, permission must be obtained from the IEEE by emailing pubs-permissions@ieee.org.

This is the author's version of an article that has been published in this journal. Changes were made to this version by the publisher prior to publication.
The final version of record is available at http://dx.doi.org/10.1109/TMTT.2014.2359855

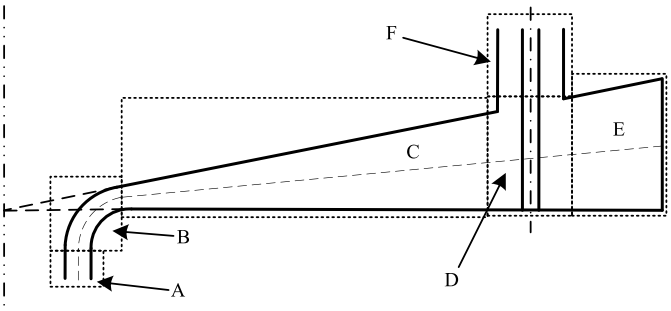

Fig. 1. Cut plane view of the basic layout of a conical line combiner showing the different regions used in the circuit model.

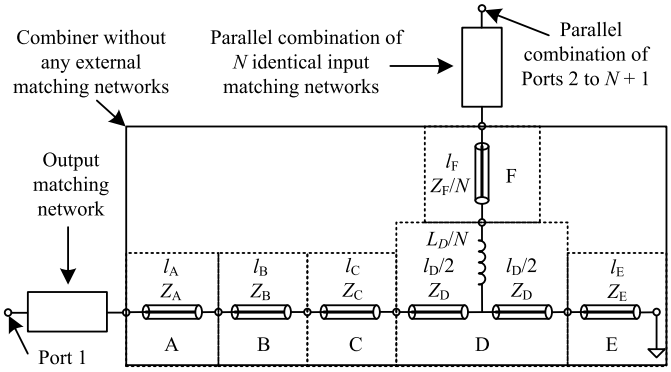

Fig. 2. Circuit model of the full combiner showing the regions corresponding to the physical model in Fig. 1, including external matching networks that may be needed.

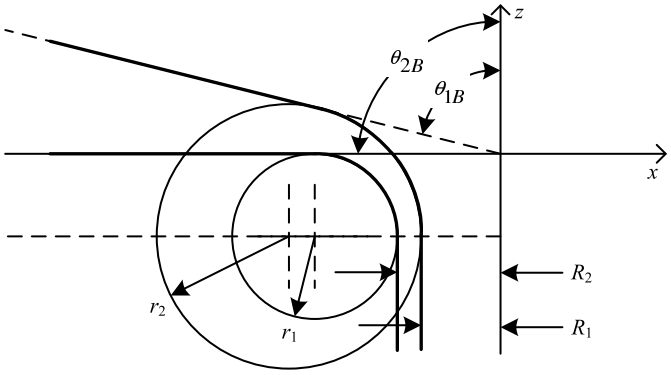

Fig. 3. A smooth conical to coaxial transmission line transition, as presented in [20].

transition, as shown in Fig. 3. These regions are all simple TEM transmission lines and can thus be modeled by ideal transmission lines with lengths and impedances derived from the physical geometry of the structure, whereas region D includes some reactive elements to compensate for the stored evanescent mode energy around the peripheral coaxial feeding port to conical line transition. Note that the transmission line in region F and the inductor in region D represent a parallel combination of N of those components for an N-way combiner.

A complete and accurate physical description of the combining structure is needed so that the transmission line lengths and impedances needed for the circuit model extraction and the circuit model based design procedures can be calculated. The equations needed for regions A, B, C, E and F will be given, followed by the extraction process for the empirical equations needed for region D. Note that no external matching networks are used during the extraction process.

A. Central Output Coaxial Line (Region A)

Region A contains a constant impedance coaxial line with inner and outer conductor radii of R_1 and R_2, respectively. The coaxial line in region A will have the same length l_A as used in the ideal transmission line model. The impedance Z_A can be calculated using

$$Z_A = 60\ln\left(\frac{R_2}{R_1}\right). \tag{1}$$

B. Central Transition (Region B)

The central transition from conical to coaxial line is designed using the smooth transition presented in [20] and shown in Fig. 3. The radii of the two arcs (r_1 and r_2) used to construct the transition are obtained using

$$r_1 = 3.5 \times (R_2 - R_1), \tag{2}$$

$$r_2 = \frac{(R_1 + r_1)\cos\theta_{1B}}{1 - \cos\theta_{1B}}, \tag{3}$$

where θ_{1B} is the conical line angle as defined in Fig. 3. The mean transmission length (the dashed line in region B, Fig. 1) can be calculated using

$$l_B = \frac{r_1 + r_2}{2} \times \frac{\theta_{2B} + \theta_{1B}}{2}, \tag{4}$$

where θ_{2B} is the conical line angle as defined in Fig. 3, and usually $\theta_{2B} = 90°$. The impedance of the transition is shown to be constant in [20] and can be determined by calculating either the coaxial or conical transmission line impedances:

$$Z_B = Z_A = 60\ln\left(\frac{R_2}{R_1}\right), \tag{5}$$

or

$$Z_B = 60\ln\left[\frac{\cot(\theta_{1B}/2)}{\cot(\theta_{2B}/2)}\right] \tag{6}$$

for air-filled coaxial and conical lines, respectively.

C. Conical Transmission Line (Region C)

The mean transmission length for this region is calculated from the edge separating regions D and C to the edge separating regions C and B. The length (the dashed line in region C, Fig. 1) can be calculated using

$$l_C = \frac{r_p}{\cos(\pi/4 - \theta_{1D}/2)} - l_n - \overline{d_s}/2, \tag{7}$$

where

$$l_n = \frac{1}{2}\left[R_1 + R_2 + r_1 + r_2\left(1 - \cos\theta_{1B}\right)\right] \tag{8}$$

is the average length of conical transmission line removed from the central part of the conical line where the transition to the central coaxial line is inserted. In (7) r_p is the peripheral

Copyright (c) 2014 IEEE. Personal use is permitted. For any other purposes, permission must be obtained from the IEEE by emailing pubs-permissions@ieee.org.

This is the author's version of an article that has been published in this journal. Changes were made to this version by the publisher prior to publication.
The final version of record is available at http://dx.doi.org/10.1109/TMTT.2014.2359855

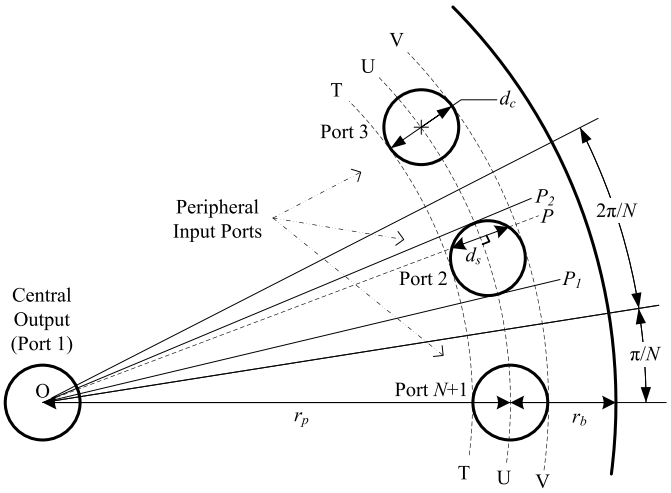

Fig. 4. A section of the combining structure showing the parts of the top conductor being removed where the coaxial lines are placed, as well as the port numbering used throughout this work.

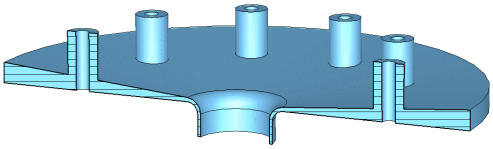

Fig. 5. The constant impedance 10-way conical combiner used to extract the model. The shaded part of the model is vacuum and the background material is perfect electrical conductor (PEC).

input port placement radius as defined in Fig. 4, $\overline{d_s}$ is the arithmetic mean of d_s in Fig. 4 as the line OP is moved from the position OP_1 to OP_2 and can be approximated using (13), and the same definition as in region B is used for θ_{1D} except that it is the angle of the conical line in region D. The length l_C is exact when region C is a constant impedance conical line, where $\theta_{1B} = \theta_{1D}$, and is a reasonable approximation if region C is an impedance tapered conical line, where $\theta_{1B} \neq \theta_{1D}$. If region C is a constant impedance conical line, then $Z_C = Z_B$, since $\theta_{1B} = \theta_{1D}$ and $\theta_{2B} = \theta_{2D} = 90°$. If region C is an impedance tapered conical line then the conical line angle θ_{1C} required to realize the desired impedance function Z_f versus distance can be approximated as a function of radial distance from the axis of symmetry of the conical line ρ, using

$$\theta_{1C}(\rho) = 2\arctan\left[\frac{\tan(\theta_{2B}/2)}{e^{Z_f(\rho - l_n)/60}}\right]. \tag{9}$$

The impedance function Z_f can be an impedance taper of the designer's choice, such as an exponential or a Hecken [21] taper.

D. Conical Transmission Line (Region E)

The length (the dashed line in region E, Fig. 1) can be calculated using

$$l_E = \frac{r_b}{\cos\left(\pi/4 - \theta_{1D}/2\right)} - \overline{d_s}/2, \tag{10}$$

where r_b is the back-short length as defined in Fig. 4. The impedance Z_E can be calculated using

$$Z_E = 60\ln\left[\frac{\cot(\theta_{1D}/2)}{\cot(\theta_{2D}/2)}\right], \tag{11}$$

since $\theta_{1D} = \theta_{1E}$ and $\theta_{2D} = \theta_{2E}$.

E. Coaxial Transmission Line (region F)

Region F contains a constant impedance coaxial line with an inner conductor radius r_{inner} and an outer conductor diameter of d_c. The coaxial line in region F will have the same length l_F as used in the ideal transmission line model. The impedance Z_F can be calculated using

$$Z_F = 60\ln\left(\frac{d_c}{2r_{inner}}\right). \tag{12}$$

F. Empirical Equation Extraction (region D)

The length l_D in the circuit model is calculated directly from the combiner dimensions, whereas empirical equations will be used to calculate the impedance Z_D and inductance L_D. The empirical equations are extracted so that they are applicable to a wide range of conical line combiners.

A sector of an N-way combiner is shown in Fig. 4 where the dimensions used to derive the expression for the length l_D are defined. The outer conductors of the peripheral ports are formed by drilling holes through one of the conical transmission line conductors and are represented by the circles between the dashed arcs T and V.

The drilling of the holes results in the removal of some of the conical line conductor, causing a change in impedance between arcs T and V. The change in impedance is approximated using two short transmission lines. It is assumed that r_p is large relative to the outer conductor diameter of the peripheral coaxial lines d_c, so that the arc U will be approximately straight inside the removed circle area. As a result, the average of d_s and thus the length l_D, can be approximated simply by using

$$l_D = \overline{d_s} = \frac{d_c\pi}{4}. \tag{13}$$

The value of Z_D is calculated by scaling the impedance of the conical transmission line to model the effect of removing some of the conductor from the conical line. This modification is expected to increase the impedance of the conical line between arcs T and V, resulting in a scaling factor for Z_D that is larger than 1. Furthermore, the value of Z_D is expected to be dependent on the ratio of the amount of conductor along the circumference of the conical line at radius r_p before the holes are made to the amount remaining after the holes are made. The empirical equation for Z_D can thus be defined as

$$Z_D = g_1(x_1)Z_{sys}, \tag{14}$$

where

$$x_1 = \frac{2\pi r_p}{2\pi r_p - N\overline{d_s}} = \frac{r_p}{r_p - \frac{Nd_c}{8}}, \tag{15}$$

Z_{sys} is the impedance of the unperturbed conical line between arcs T and V before the peripheral ports are inserted

Copyright (c) 2014 IEEE. Personal use is permitted. For any other purposes, permission must be obtained from the IEEE by emailing pubs-permissions@ieee.org.

This is the author's version of an article that has been published in this journal. Changes were made to this version by the publisher prior to publication.
The final version of record is available at http://dx.doi.org/10.1109/TMTT.2014.2359855

TABLE I
EXTRACTED POLYNOMIALS FOR THE EMPIRICAL EQUATIONS

Function	Units
$g_1(x_1, \Delta r) = -0.054x_1\Delta r + 0.48x_1 + 0.072\Delta r + 0.38$	Ω/Ω
$g_2(x_2, \Delta r) = 62x_2\Delta r + 320x_2 - 230\Delta r - 5.7$	pH

($Z_{sys} = Z_E$), and N is the number of peripheral feeding ports of the combiner.

The inductor in region D models the extended center conductor pin of the peripheral coaxial lines and its value is expected to be dependent on the pin length. Thus,

$$L_D = g_2(x_2), \tag{16}$$

where

$$x_2 = r_p \cot\theta_{1D} \tag{17}$$

is the length of the coaxial pin extending into the conical transmission line.

A simple constant impedance conical combiner as shown in Fig. 5 is used to extract the empirical equations that describe Z_D and L_D. This is done by fitting the scattering parameters of the circuit model onto the corresponding ones produced by full-wave simulations. All full-wave simulations are performed using the time domain solver in Computer Simulation Technology (CST) Microwave Studio (MWS) [22]. A mean square error function is defined in order to measure how well the model matches the full-wave simulations:

$$\varepsilon = \sum_{k=1}^{K} \frac{1}{K} |S_{11}^f(f_k) - S_{11}^c(f_k)|^2 \ . \tag{18}$$

S_{11}^f and S_{11}^c are the S-Parameters of the full-wave and circuit simulations, respectively, and f_k is the kth frequency sample of a total of K samples. Port 1 is the central port and ports 2 to $N+1$ are the peripheral ports, as defined in Fig. 4. A Nelder-Meade based Simplex search [23] is used to minimize ε over a wide bandwidth ($> 100\%$) around a chosen center frequency by adjusting the values of Z_D and L_D in the circuit model. The center frequency is determined by the length of the back-short in the conical line r_b (also defined in Fig. 4), which is equal to a quarter wavelength at that frequency. A center frequency of 10 GHz is used to extract the empirical equations. Straight lines fit the resulting values of Z_D and L_D well, however, the coefficients of the best fitting lines change for different peripheral port dimensions. A straight line is thus fitted to each set of data points sharing the same peripheral port dimensions, resulting in a number of different equations. These equations are combined by fitting polynomials to the obtained coefficients for different peripheral port dimensions versus Δr, with

$$\Delta r = d_c/2 - r_{\text{inner}}, \tag{19}$$

where r_{inner} is the inner conductor radius, and d_c is the outer conductor diameter of the peripheral coaxial feeding ports. The resulting empirical equations are the simple bivariate polynomials given in Table I. Note that all dimensions should be specified in millimeters.

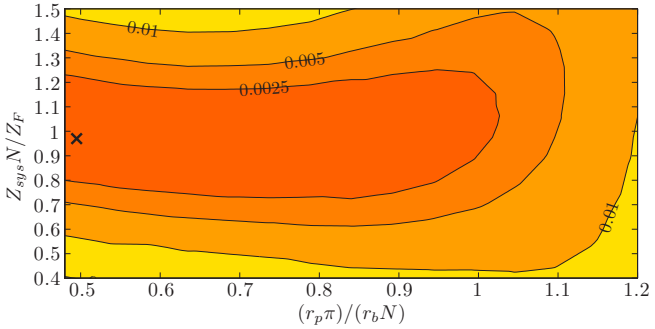

(a) 10 GHz (X-Band) combiners with 3.5 mm peripheral ports.

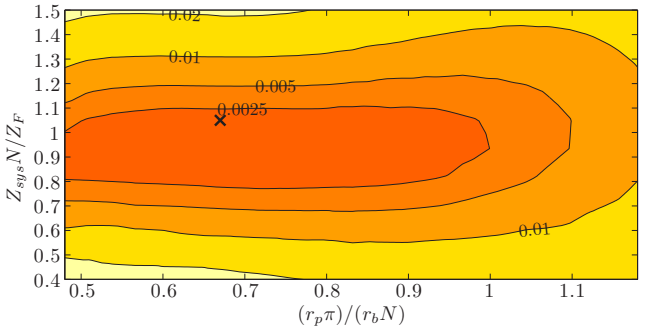

(b) 10 GHz (X-Band) combiners with 85.6 Ω peripheral ports with SubMiniature version A (SMA) connector inner conductor dimensions.

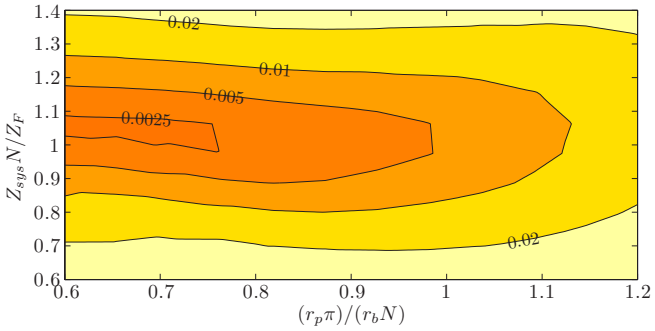

(c) 10 GHz (X-Band) combiners with N-type peripheral ports.

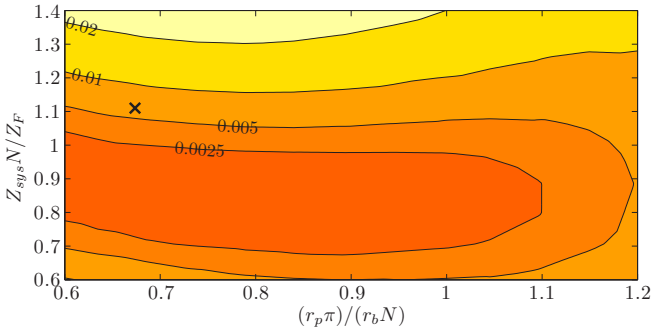

(d) 6 GHz (C-Band) combiners with N-type peripheral ports.

Fig. 6. Contour plots of the mean square error, as defined in (18), between full-wave simulations and their equivalent circuit models. The accuracy of the circuit models used for the designs in section V are indicated by ×-markers on the contour plots: The 30 port X-Band combiner is shown in (a), the 10 port X-Band combiner in (b) and the 15 port C-Band combiner in (d).

Copyright (c) 2014 IEEE. Personal use is permitted. For any other purposes, permission must be obtained from the IEEE by emailing pubs-permissions@ieee.org.

This is the author's version of an article that has been published in this journal. Changes were made to this version by the publisher prior to publication.
The final version of record is available at http://dx.doi.org/10.1109/TMTT.2014.2359855

III. Parameter Study

A parameter study is performed to test the accuracy of the model. Equivalent circuit models for various combiners are built using the information presented in Section II (a detailed design procedure is given in Section IV). Combiners with center frequencies of 6 GHz (C-Band) and 10 GHz (X-Band) and peripheral feeding ports with the same inner and outer conductor radii as the standard 50 Ω 3.5 mm and N-type connectors are used to generate the data shown in Fig. 6. A combiner with 85.6 Ω peripheral feeding ports with the same inner conductor radius as the standard SubMiniature version A (SMA) connector is also used, similar to what is used in [11], with a different outer conductor radius from the standard 50 Ω SMA connector. The quantities Z_{sys}, Z_F, N, r_p, and r_b in Fig. 6 are defined in Section II.

The error function defined in (18) is used to show how well the scattering parameters of the circuits match their corresponding full-wave simulations for different combiner dimensions over a larger than 100% bandwidth. These contour plots may be of interest to the designer when using the model. The need for full-wave simulations can be eliminated by limiting the combiner dimensions to regions where ε is small, however this model could still serve well as a coarse model for space mapping techniques in situations where the combiner dimensions cannot be limited to the higher accuracy regions, or when the results are not satisfactory.

Fig. 6 has been generated using data for 10-way combiners. However, similar data for 15-way and 20-way combiners with 85.6 Ω SMA feeding ports has been generated and compared to the data for $N = 10$. A statistical analysis of the data reveals that the model accuracy is relatively independent of N: The mean error function variance for the three values of N is

$$\mathrm{Var}(\varepsilon)_{\mathrm{mean}} = 3.19 \times 10^{-7}, \tag{20}$$

and the maximum error function variance is

$$\mathrm{Var}(\varepsilon)_{\mathrm{max}} = 1.42 \times 10^{-5}. \tag{21}$$

A comparison of the results for combiners with N-type ports operating at X-Band [Fig. 6(c)], where $d_c/r_b \approx 0.9$, and at C-Band [Fig. 6(d)], where $d_c/r_b \approx 0.5$, shows that the electrical size of the peripheral ports influences the accuracy of the circuit model: The region with higher accuracy ($\varepsilon < 2.5 \times 10^{-3}$) is much larger at C-Band than at X-Band. The same effect can be seen by comparing Figs. 6(a) and 6(c), which are for combiners with the same center frequency, but with different peripheral port sizes. As a general rule, the outer conductor diameter of the peripheral ports should be less than a quarter of a wavelength at the center frequency, thus $d_c/r_b < 1$, and increased accuracy is expected for smaller diameters.

IV. Design Procedure

The physical description, equivalent circuit model, and empirical equations presented in Section II are used to compile a step-by-step design procedure so that the designer may use the presented information in a systematic way. The number of input ports N, the wavelength at the center frequency of the operating band λ_c, and the type of connectors to be used for the peripheral input ports and central output port should be selected before starting the design procedure. The first part of the design consists of setting up initial values and/or constraints for the parameters that can be optimized. The optimizable parameters are all either physical dimensions or can be directly related to physical dimensions of the combiner. The parameter study performed in Section III is used to create a set of recommendations that will assist the designer in obtaining more accurate results. The second part of the design consists of analyzing and optimizing the equivalent circuit model for one or more design goals. When satisfactory results are obtained, a 3D model of the combiner may be constructed and a single analysis performed using full-wave simulation software, such as CST MWS, in order to verify the design.

A. Recommended initial values or constraints for optimizable parameters

1) For the back-short length r_b, it is recommended that
$$r_b \approx \frac{\lambda_c}{4}. \tag{22}$$
2) For the outer conductor diameter d_c, of the peripheral input coaxial lines it is recommended that
$$d_c < r_b. \tag{23}$$
Consider that the coaxial lines modeled by region F need to interface with matching networks or – if the matching networks are omitted – directly with the input connectors. Calculate the resulting values for Z_F using d_c and the radius of the inner conductor r_{inner} that will be used for the peripheral input ports using (12).
3) It is recommended, in general, that for the impedance of the unperturbed conical line in region D, as described in Section II,
$$Z_{sys} \approx \frac{Z_F}{N}. \tag{24}$$
4) For the peripheral input port placement radius r_p, improved accuracy of the circuit model can be obtained, in general, when
$$r_p < \frac{N r_b}{\pi}, \tag{25}$$
while also keeping r_p large enough to accommodate all of the input connectors for ports 2 to $N + 1$.
5) For the outer conductor radius R_2 of the coaxial line in region A, the fact that this coaxial line will need to interface either directly with the chosen output connector or with an output matching network should be taken into consideration.
6) The inner conductor radius R_1 of the coaxial line in region A also affects the conical to coaxial line transition in region B, since $Z_A = Z_B$. Furthermore, if region C is a constant impedance conical line, then $Z_A = Z_B = Z_C = Z_{sys} = Z_E$. However, using a constant impedance conical line in region C may lead to manufacturing difficulties and inaccuracies due to the small spacing $(R_2 - R_1)$ that is required in order to realize a low impedance coaxial transmission line, as pointed out in [11]. It is thus recommended

Copyright (c) 2014 IEEE. Personal use is permitted. For any other purposes, permission must be obtained from the IEEE by emailing pubs-permissions@ieee.org.

This is the author's version of an article that has been published in this journal. Changes were made to this version by the publisher prior to publication.
The final version of record is available at http://dx.doi.org/10.1109/TMTT.2014.2359855

to use a tapered conical line in region C that tapers the impedance from Z_{sys} up to a higher impedance in regions A and B, resulting in a larger spacing and thus improved manufacturability. In this case R_1 is chosen or optimized and constrained to provide adequate spacing, and r_p will affect the taper length.

B. Calculation of equivalent circuit model element values

The equivalent circuit model of the entire combining structure, as shown in Fig. 2, can now be constructed in a circuit simulator. Fig. 2 shows the location of external matching networks, for example stepped impedance coaxial lines, that may be added by the designer. The designer will need to find or derive the equivalent circuit models for any added external matching networks needed for a specific combiner design. The circuit element values of the equivalent model can now be calculated using the parameters described in Section IV-A as variables, by using the following procedure:

1) Calculate Z_B from (5).
2) Calculate θ_{1B} using (6) where typically $\theta_{2B} = 90°$.
3) l_B can be calculated using (4).
4) l_A can be optimized together with an external output matching network, or if region A is already matched to the desired output port impedance and dimensions, l_A can be zero.
5) $Z_A = Z_B$.
6) l_C can be calculated using (7).
7) If region C is a constant impedance conical line then $Z_C = Z_B$, otherwise the profile of the desired impedance taper, such as an exponential or a Hecken [21] taper, with a length of l_C should be calculated using (9).
8) Calculate Δr using (19).
9) l_D can be calculated using (13).
10) Z_D can be calculated by combining (14), (15), and the function $g_1(x_1, \Delta r)$ listed in Table I.
11) Calculate θ_{1D} using (11) where typically $\theta_{2D} = 90°$.
12) L_D can be calculated by combining (16), (17), and the function $g_2(x_1, \Delta r)$ listed in Table I.
13) l_E can be calculated using (10).
14) $Z_E = Z_{sys}$, and thus with $\theta_{2E} = \theta_{2D}$, $\theta_{1E} = \theta_{1D}$.
15) l_F can be optimized together with an external input matching network, or if region F is already matched to the desired input port impedance and dimensions, l_F can be zero.
16) Z_F can be calculated using (12).

The entire circuit model including external matching networks and the impedance tapered conical line in region C can now be optimized for one or more chosen design goals.

V. Design Examples

The circuit model is further validated by completing some example designs with external input and output matching networks and comparing the S-parameters of the model with the full-wave simulations. Three different combiners are designed with stepped impedance central coaxial ports to match them to 50 Ω, similar to the combiner in [10], using [24] to calculate

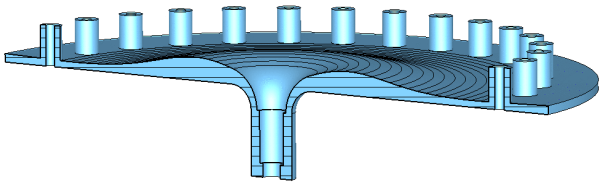

(a)

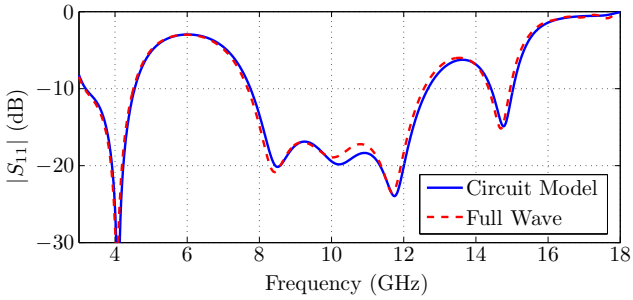

(b)

Fig. 7. (a) The full-wave simulation model of the 30-way X-Band combiner with standard 3.5 mm connector dimension peripheral ports, and (b) the comparison between the full-wave and equivalent circuit model output port reflection coefficients (S_{11}).

the step capacitances. In each of the combiners, the impedance of the conical lines are tapered up to higher values near the central port, as is done in [11], except that a smooth Hecken taper [21] is used instead of a Klopfenstein taper [25]. These examples also serve as an indication of how well the circuit model S-Parameters match the full-wave simulations for combiners that fall into different accuracy regions as shown in Fig. 6 and explained in section III.

The first design is for an X-Band 30-way combiner, with a center frequency of 10 GHz, that has 50 Ω peripheral ports with the same inner conductor radius as the standard 3.5 mm connector. The 3D model used for the full-wave simulation is shown in Fig. 7(a), and excellent agreement between the circuit model and full-wave simulation is shown in Fig. 7(b). This level of accuracy is achieved by limiting the combiner dimensions to the higher accuracy and thus lower error regions as indicated by the ×-marker in Fig. 6(a).

The second design is for a C-Band 15-way combiner, shown in Fig. 8(a), with a center frequency of 6 GHz and 50 Ω peripheral ports with inner conductor radii corresponding to the standard N-type connector dimensions. A comparison between the circuit model and full-wave simulation results is shown in Fig. 8(b), with slightly deteriorated but still good agreement considering that this combiner falls into a much lower accuracy region [see Fig. 6(d)] compared to the previous design. This example demonstrates that the model is valid for a different frequency range.

The third design is for an X-Band 10-way combiner, with a center frequency of 10 GHz, that has stepped impedance peripheral ports with a constant inner conductor radius equal to that of the standard SMA connector. The peripheral ports are stepped into a 65.4 Ω partially filled coaxial transmission line followed by a 85.6 Ω section that transitions into the conical transmission line, as shown in Fig. 9(a). This is similar

Copyright (c) 2014 IEEE. Personal use is permitted. For any other purposes, permission must be obtained from the IEEE by emailing pubs-permissions@ieee.org.

This is the author's version of an article that has been published in this journal. Changes were made to this version by the publisher prior to publication.
The final version of record is available at http://dx.doi.org/10.1109/TMTT.2014.2359855

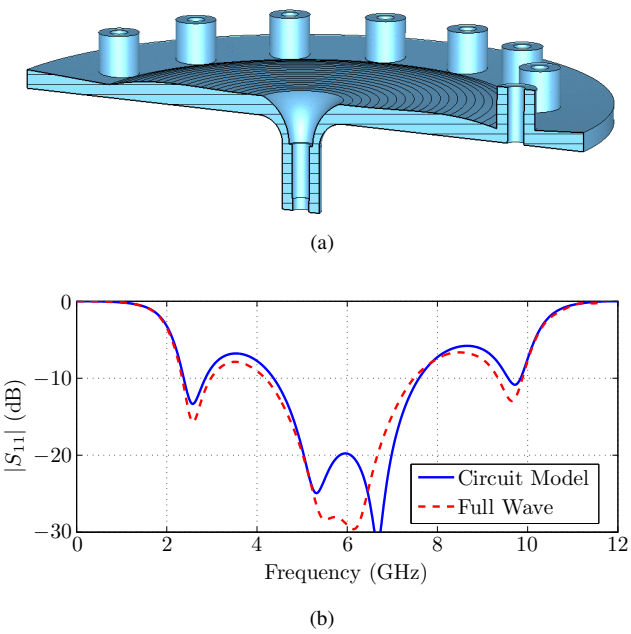

Fig. 8. (a) The full-wave simulation model of the 15-way X-Band combiner with standard N-type connector dimension peripheral ports, and (b) the comparison between the full-wave and equivalent circuit model output port reflection coefficients (S_{11}).

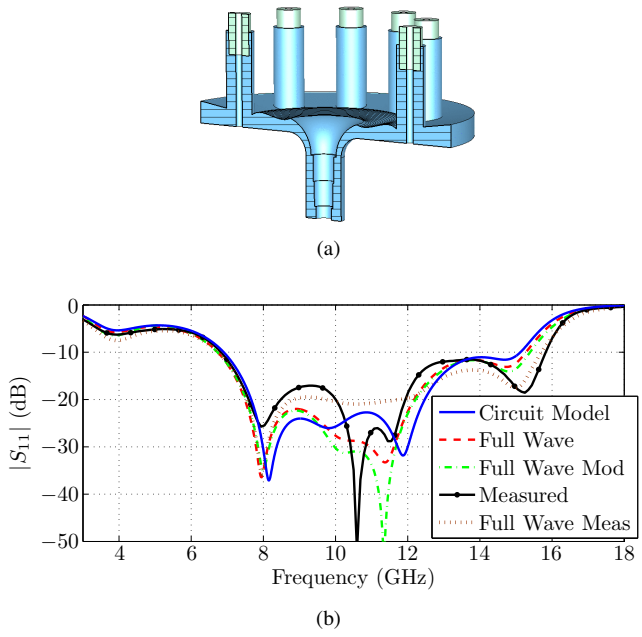

Fig. 9. (a) The full-wave simulation model of the 10-way X-Band combiner with standard SMA connector dimension peripheral ports, and (b) the comparison between the circuit model, full-wave, modified full-wave and measured output port reflection coefficients (S_{11}). The full-wave simulated S_{11} using the measured profile of the manufactured combiner (shown in Fig. 10) is also shown in (b).

to the peripheral ports used in [11]. The stepped impedance feeding lines add degrees of freedom, namely the lengths of the 65.4 Ω (l_{par}) and 85.6 Ω (l_F) lines, that can be optimized. The impedance step introduces a small shunt capacitance that can be omitted due to its small effect. The central port reflection coefficient (S_{11}) is shown in Fig. 9(b) and the circuit model is in excellent agreement with the full-wave simulation. For this design $r_p + r_b = 25.9$ mm compared to $r_p + r_b = 40$ mm in [11], while exhibiting similar performance. The reduction in size is mainly due the fact that the impedance taper in the conical line no longer needs to be designed as in [11], where the taper length is maximized in order to achieve the best possible reflection coefficient in the passband. This was required since the combining structure, and thus the taper, was not included in the optimization parameter space since full-wave analysis was used to find the response. The circuit model approach used here allows the taper to be optimized together with the impedance levels and transmission line lengths throughout the entire combiner, and it can consequently have a shorter length. The final parameters of the optimized combiner are: $R_2 = 3.5$ mm, $Z_A = Z_B = 20.18$ Ω, $l_A = 0$, $Z_E = Z_{sys} = 9$ Ω, $d_c = 5.164$ mm, $r_{inner} = 0.62$ mm, $r_p = 17$ mm, $r_b = 7.9$ mm, $Z_F = 85.6$ Ω, $l_F = 9.5$ mm, $l_{par} = 4$ mm. The stepped coaxial output matching network has impedance levels of 32.89 Ω and 38.62 Ω, and lengths of 4.4 mm and 4.2 mm, in that order, followed by a 50 Ω coaxial line. The Hecken taper in region C has $B = 0 + j2.47$, with B defined in [21]. This design is chosen for construction and measurement.

VI. Construction and Measurements

A computer numerically controled (CNC) lathe is usually able to machine conical structures, such as conical transmission lines, with ease. There are, however, a few limitations that need to be considered. The finite radius of the cutting tool tip limits the size of the smallest concave feature of the structure. The tool tip radius is taken into account by blending all concave corners with a radius equal to or larger than the tip radius. For this design, this modification has very little effect on the combiner performance, since the tip radius (0.4 mm in this case) is much smaller than the guided wavelength at X-Band ($\lambda_g \approx 30$ mm). Additionally, all the areas in the combiner requiring this modification have relatively low local field intensities, further reducing its effect. For full-wave simulation purposes, the impedance taper in the conical line is defined by a series of coordinates connected by short straight lines. For construction, the impedance taper is much more conveniently defined by a series of tangential circle sections passing through or near the series of coordinates. The full-wave simulation results of the modified combiner in Fig. 9(b) show that while these modifications significantly reduce the manufacturing effort, the combiner performance is barely affected at all.

The size, shape, and angle of the cutting tool holder and/or toolpost that is used imposes limitations on the realizable shape of the structure. The goal is to use the least number of different cutting tools, since each interchanging of tools increases the cost and introduces a degree of uncertainty, as well as visible and often palpable step discontinuities. If necessary, it is desirable to change the cutting tool at a large radius in this type of structure, since any discontinuities or uncertainties will have less of an effect where the energy is spatially more dispersed. The shape and angle of the cutting tool also influences the amount of effort needed during

Copyright (c) 2014 IEEE. Personal use is permitted. For any other purposes, permission must be obtained from the IEEE by emailing pubs-permissions@ieee.org.

This is the author's version of an article that has been published in this journal. Changes were made to this version by the publisher prior to publication.
The final version of record is available at http://dx.doi.org/10.1109/TMTT.2014.2359855

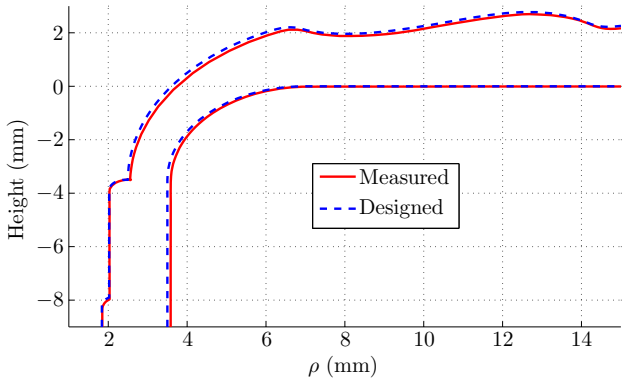

(a)

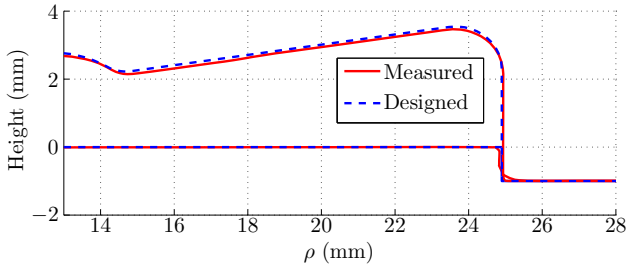

(b)

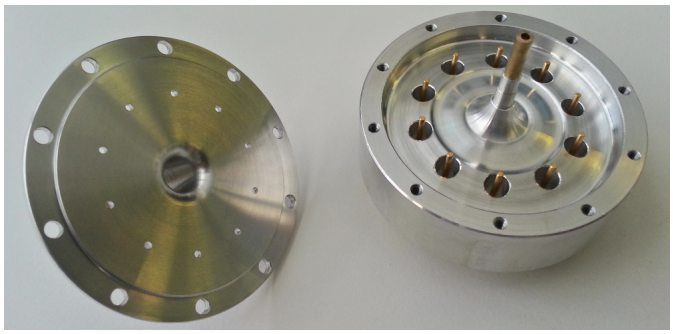

(c)

Fig. 10. The measured profile of the manufactured device is compared to the CAD model dimensions in (a) and (b), and a photo of the manufactured top and bottom halves of the combiner is shown in (c).

fabrication and whether a certain shape is realisable at all. For example, if the structure has a profile that does not increase or decrease monotonically in height versus radius, as is the case with the chosen design example, the cutting tool needs to be sufficiently narrow and its holder appropriately shaped so that it has enough clearance of the rest of the structure at all times.

The profile of the machined part is measured and compared to the 3D CAD model dimensions in Fig. 10 showing excellent agreement with the design. The largest errors can be seen in the coaxial to conical transition and the impedance taper in the conical line. A photo of the manufactured top and bottom halves of the combiner is shown in Fig. 10(c).

The measured central port reflection coefficient and peripheral port isolation are shown in Figs. 9(b) and 11 and are in good agreement with their simulated values. A full-wave

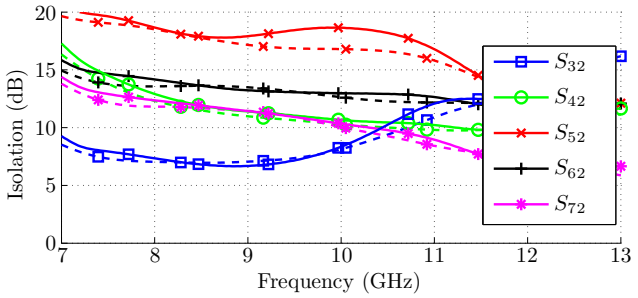

(a)

Fig. 11. The full-wave simulated isolation (dashed lines) compared to the measured isolation (solid lines) of the combiner in its operating band.

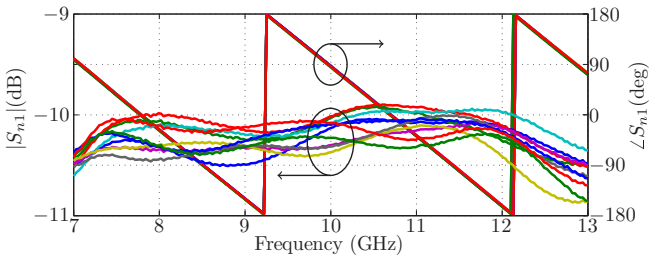

(a)

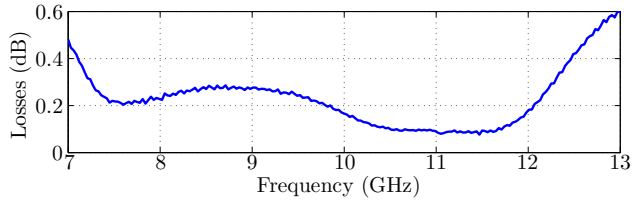

(b)

Fig. 12. The measured phase and amplitude balance is shown in (a), where n is the peripheral port number with $n = 2, ..., N + 1$. The total insertion loss of the combiner is shown in (b).

TABLE II
COMPARISON WITH OTHER RECENT WORK

Ref.	Type	N	Return Loss (dB)	Bandwidth	Frequency Band
This Work	Conical	10	18	46%	X-Band
[11]	Conical	10	18.5	47%	X-Band
[10]	Conical	10	14.7	74%	X-Band
[9]	Radial	30	14	15%	Ku-Band
[15]	Radial	10	15	35%	Ku-Band
[12]	Coaxial	8	12	112%	L-Band
[13]	Coaxial	10	15	30%	Ku-Band

simulation is performed using the measured dimensions of the manufactured combiner and the resulting central port reflection coefficient is shown in Fig. 9(b). The remaining difference between the measured and simulated S_{11} could be due to a number of factors, such as the SMA to N-type adapter or the non-ideal SMA terminations used during the measurements.

The central port return loss and fractional bandwidth is shown in Table II for comparison with other work. The measured peripheral port isolation is better than 6 dB compared to roughly 6 dB in [11] and 5 dB in [10]. The measured amplitude

Copyright (c) 2014 IEEE. Personal use is permitted. For any other purposes, permission must be obtained from the IEEE by emailing pubs-permissions@ieee.org.

This is the author's version of an article that has been published in this journal. Changes were made to this version by the publisher prior to publication.
The final version of record is available at http://dx.doi.org/10.1109/TMTT.2014.2359855

and phase balance is shown in Fig. 12(a). The maximum measured amplitude and phase imbalance is $\pm$ 0.6 dB and $\pm$ 3°, respectively, versus $\pm$ 0.7 dB and $\pm$ 5° in [11], and $\pm$ 1.5 dB and $\pm$ 10° in [10]. The insertion loss shown in Fig. 12(b) is calculated by substituting the measured values for S_{j1}, $j = 2, 3, ..., N+1$ into

$$Losses = -10\log_{10}\left(\sum_{j=2}^{N+1}|S_{j1}|^2\right). \quad (26)$$

The maximum insertion loss in the operating band is 0.28 dB, which is the same as in [11], and an improvement compared to [10], where a stepped impedance matching network is used.

VII. Conclusion

A simple equivalent circuit model has been presented together with empirical equations that allow for rapid circuit based design and optimization of conical power combiners with shorted coaxial feed ports. The results of a parametric study on the accuracy of the circuit model are presented in a format that may be helpful to the designer. The effectiveness of the circuit model has been demonstrated by using it to design a significantly smaller combiner with performance comparable to previously published designs. The manufactured design exhibits excellent agreement with the circuit model and full-wave simulations.

Acknowledgment

The authors would like to thank Comar International and Reutech Radar Systems (Pty) Ltd. in Stellenbosch, South Africa for assistance in manufacturing and financial support of the project.

References

[1] K. J. Russell, "Microwave power combining techniques," *IEEE Trans. Microw. Theory Techn.*, vol. 27, no. 5, pp. 472–478, May 1979.
[2] K. Chang and C. Sun, "Millimeter-wave power-combining techniques," *IEEE Trans. Microw. Theory Techn.*, vol. 31, no. 2, pp. 91–107, Feb. 1983.
[3] R. A. York, "Some considerations for optimal efficiency and low noise in large power combiners," *IEEE Trans. Microw. Theory Techn.*, vol. 49, no. 8, pp. 1477–1482, Aug. 2001.
[4] M. E. Bialkowski and V. P. Waris, "Electromagnetic model of a planar radial-waveguide divider/combiner incorporating probes," *IEEE Trans. Microw. Theory Techn.*, vol. 41, no. 6, pp. 1126–1134, Jun. 1993.
[5] T.-I. Hsu and M. D. Simonutti, "A wideband 60 GHz 16-way power divider/combiner network," in *IEEE MTT-S Int. Microw. Symp. Dig.*, May 1984, pp. 175–177.
[6] R. Harp and H. Stover, "Power combining of X-band IMPATT circuit modules," in *IEEE Int. Solid-State Circuits Dig. Tech. Pap.*, vol. XVI, Feb. 1973, pp. 118–119.
[7] R. Mellavarpu and G. MacMaster, "500 MHz, 100 W X-band solid state amplifier," in *IEEE MTT-S Int. Microw. Symp. Dig.*, Jun. 1985, pp. 387–390.
[8] J. P. Quine, J. G. McMullen, and D. D. Khandelwal, "Ku-band IMPATT amplifiers and power combiners," in *IEEE-MTT-S Int. Microw. Symp. Dig.*, Jun. 1978, pp. 346–348.
[9] A. E. Fathy, S.-W. Lee, and D. Kalokitis, "A simplified design approach for radial power combiners," *IEEE Trans. Microw. Theory Techn.*, vol. 54, no. 1, pp. 247–255, Jan. 2006.
[10] D. I. L. de Villiers, P. W. van der Walt, and P. Meyer, "Design of a ten-way conical transmission line power combiner," *IEEE Trans. Microw. Theory Techn.*, vol. 55, no. 2, pp. 302–308, Feb. 2007.
[11] D. I. L. de Villiers, P. W. van der Walt, and P. Meyer, "Design of conical transmission line power combiners using tapered line matching sections," *IEEE Trans. Microw. Theory Techn.*, vol. 56, no. 6, pp. 1478–1484, Jun. 2008.
[12] M. Amjadi and E. Jafari, "Design of a broadband eight-way coaxial waveguide power combiner," *IEEE Trans. Microw. Theory Techn.*, vol. 60, no. 1, pp. 39–45, Jan. 2012.
[13] K. Song and Q. Xue, "Planar probe coaxial-waveguide power combiner/divider," *IEEE Trans. Microw. Theory Techn.*, vol. 57, no. 11, pp. 2761–2767, Nov. 2009.
[14] ——, "Ultra-wideband ring-cavity multiple-way parallel power divider," *IEEE Trans. Ind. Electron.*, vol. 60, no. 10, pp. 4737–4745, Oct. 2013.
[15] K. Song, F. Zhang, S. Hu, and Y. Fan, "Ku-band 200-W Pulsed power amplifier based on waveguide spatially power-combining technique for industrial applications," *IEEE Trans. Ind. Electron.*, vol. 61, no. 8, pp. 4274–4280, Aug. 2014.
[16] Q. Xue, K. Song, and C.-H. Chan, "China: Power combiners/dividers," *IEEE Microwave Magazine*, vol. 12, no. 3, pp. 96–106, May 2011.
[17] D. I. L. de Villiers, "A simplified peripheral feeding network for conical line power combiners," in *Proc. Asia-Pacific Microw. Conf.*, Dec. 2012, pp. 986–988.
[18] G. W. Swift and D. I. Stones, "A comprehensive design technique for the radial wave power combiner," in *IEEE MTT-S Int. Microw. Symp. Dig.*, May 1988, pp. 279–281.
[19] R. D. Beyers and D. I. L. de Villiers, "Analysis of shorted coaxial peripheral feeding networks for conical line power combiners," in *Proc. Asia-Pacific Microw. Conf.*, Nov. 2013, pp. 285–287.
[20] P. W. der Walt, "A novel matched conical line to coaxial line transition," in *Proc. South African Commun. Signal Process. Symp.*, Sep. 1998, pp. 431–434.
[21] R. P. Hecken, "A near-optimum matching section without discontinuities," *IEEE Trans. Microw. Theory Techn.*, vol. 20, no. 11, pp. 734–739, Nov. 1972.
[22] Computer Simulation Technology, CST Studio Suite 2011, Darmstadt, Germany. [Online]. Available: http://www.cst.com
[23] J. A. Nelder and R. Mead, "A simplex method for function minimization," *Comput. J.*, vol. 7, no. 4, pp. 308–313, 1965.
[24] P. I. Somlo, "The Computation of Coaxial Line Step Capacitances," *IEEE Trans. Microw. Theory Techn.*, vol. 15, no. 1, pp. 48–53, Jan. 1967.
[25] R. W. Klopfenstein, "A transmission line taper of improved design," *Proc. IRE*, vol. 44, no. 1, pp. 31–35, Jan. 1956.

Ryno D. Beyers (S'13) was born in Bellville, South Africa, on April 22, 1989. He received the B.Eng degree in electrical and electronic engineering from the University of Stellenbosch, Stellenbosch, South Africa, in 2011, and is currently working towards the Ph.D. degree in electrical and electronic engineering at the University of Stellenbosch.

His current research interests include passive devices and network synthesis.

Dirk I. L. de Villiers (S'05-M'08) was born in Langebaan, South Africa, on October 13, 1982. He received the B.Eng and Ph.D. degrees in electrical and electronic engineering from the University of Stellenbosch, Stellenbosch, South Africa in 2004 and 2007 respectively. During 2005 to 2007 he spent several months as visiting researcher with the Computational Modeling and Programming group at the University of Antwerp in Antwerp, Belgium.

From 2008 to 2009 he was a post-doctoral fellow at the University of Stellenbosch working on antenna feeds for the South African SKA program. During this time he was also a part time lecturer at the Cape Peninsula University of Technology. He is currently a senior lecturer at the University of Stellenbosch, and his main research interests include reflector antennas as well as the design of wide band microwave components such as combiners, filters, and antennas.

Copyright (c) 2014 IEEE. Personal use is permitted. For any other purposes, permission must be obtained from the IEEE by emailing pubs-permissions@ieee.org.